ELSEVIER

Agricultural and Forest Meteorology 110 (2002) 177–201

AGRICULTURAL AND FOREST METEOROLOGY

www.elsevier.com/locate/agrformet

Energy budget above a high-elevation subalpine forest in complex topography

A.A. Turnipseed [a,*], P.D. Blanken [b], D.E. Anderson [c], R.K. Monson [a,d]

[a] *Department of Environmental, Population and Organismic Biology, Campus Box 334, University of Colorado, Boulder, CO 80309, USA*
[b] *Department of Geography, Campus Box 260, University of Colorado, Boulder, CO 80309, USA*
[c] *Water Resources Division, Denver Federal Center, US Geological Survey, Box 25046, Mail Stop 413, Building 53, Lakewood, CO 80225, USA*
[d] *Cooperative Institute for Research in Environmental Sciences (CIRES), University of Colorado, Boulder, CO 80309, USA*

Received 27 June 2001; received in revised form 13 November 2001; accepted 18 November 2001

Abstract

Components of the energy budget were measured above a subalpine coniferous forest over two complete annual cycles. Sensible and latent heat fluxes were measured by eddy covariance. Bowen ratios ranged from 0.7 to 2.5 in the summer (June–September) depending upon the availability of soil water, but were considerably higher (∼3–6) during winter (December–March). Energy budget closure averaged better than 84% on a half-hourly basis in both seasons with slightly greater closure during the winter months. The energy budget showed a dependence on friction velocity (u^*), approaching complete closure at u^* values greater than 1 m s^{-1}. The dependence of budget closure on u^* explained why energy balance was slightly better in the winter as opposed to summer, since numerous periods of high turbulence occur in winter. It also explained the lower degree of energy closure (∼10% less) during easterly upslope flow since these periods were characterized by low wind speeds ($U < 4$ m s^{-1}) and friction velocities ($u^* < 0.5$ m s^{-1}). Co-spectral analysis suggests a shift of flux density towards higher frequencies under conditions where closure was obtained. It is suggested that low frequency contributions to the flux and advection were responsible for the lack of day-time energy budget closure. These effects were reduced at high friction velocities observed at our site. Our ability to close the energy budget at night was also highly dependent on friction velocity, approaching near closure (∼90%) at u^* values between 0.7 and 1.1 m s^{-1}. Below this range, the airflow within the canopy becomes decoupled with the flow above. Above this range, insufficient temperature resolution of the sonic anemometer obscured the small temperature fluctuations, rendering measurements intractable.

Keywords: Energy budget; Sensible heat flux; Latent heat flux; Eddy covariance; Coniferous forest

1. Introduction

Montane and subalpine forests in the western United States provide critical natural resources in a region that is undergoing rapid population increase. They help reduce the rate of spring snowmelt and aid in the infiltration of surface water into soils at high-elevations, thus, playing a key role in the regional hydrology, which has a direct impact on water availability and use. The partitioning of energy within these forest ecosystems has a direct bearing on forest hydrology, including the timing of the spring snowmelt, the accumulation of snow over the winter, and the water status of the forest and soils through the growing season.

* Corresponding author. Fax: +303-492-8699.
E-mail addresses: aturnip@colorado.edu (A.A. Turnipseed), blanken@spot.colorado.edu (P.D. Blanken), deander@usgs.gov (D.E. Anderson), monsonr@colorado.edu (R.K. Monson).

0168-1923/02/$ – see front matter
PII: S0168-1923(01)00290-8

Since high-elevation forests are often in rough terrain, their study has been hindered due to the limited number of tractable methods capable of assessing flux. Measurements at the leaf, branch or tree scale are suitable in such environments; yet do not integrate over large areas, as do micrometeorological methods such as eddy covariance. The use of micrometeorological-based methods has been thought to be unacceptable due to the complexities of the streamline flow and advection brought about by the uneven topography. These complexities may result in violations of the underlying assumptions inherent in the methodology. However, recent work has shown that the eddy covariance technique can provide a measurement that is representative of the surrounding area even under non-ideal topography or above complex canopies. Numerous studies have emerged indicating that the technique can be extended to study trace gas exchange over more complicated forested sites in more challenging terrain (Goulden et al., 1996; Greco and Baldocchi, 1996; Jarvis et al., 1997; Blanken et al., 1998; Anthoni et al., 1999; Aubinet et al., 2000). Eddy covariance provides a way to independently measure the fluxes of energy into and out of the ecosystem. Measurement and balancing of all the energy input and output terms provides a rigorous test of the eddy covariance method. For example, the sum of the turbulent fluxes of sensible (H) and latent heat (λE) should be balanced by or equal to the non-turbulent fluxes (e.g. $R_{net} - G - S_T$, where R_{net} is the net radiation, G the soil heat flux, and S_T the total heat storage between the surface and the measurement height). The degree to which these terms do not balance (i.e. lack of closure) indicates either (1) omission of an energy balance term and/or (2) unaccounted error in the measurement of at least one energy balance term. However, it has been observed that a complete energy balance is rarely (if ever) attained, even at relatively uncomplicated sites (Goulden et al., 1996, 1997; Blanken et al., 1997, 1998; Mahrt, 1998; Wilson et al., 2001). Whereas incomplete energy balance is understandable under certain circumstances (i.e. high atmospheric stability at night which leads to reduced vertical transport), other reasons for lack of closure are unresolved.

In this paper, we describe the measurements needed to evaluate the energy budget over a subalpine forest situated in complex topography. The Niwot Ridge AmeriFlux (see Hollinger and Wofsy, 1997 for AmeriFlux description) site is located in a high-elevation, subalpine forest. Measurements of the turbulent fluxes of momentum, heat, water vapor, and CO_2 by eddy covariance have been ongoing since November, 1998. Complete measurements of the energy budget components began in July 1999. This site is complicated both by sloping topography and a complex forest ecosystem. Because of its high-elevation and proximity to much higher mountains (∼8 km to the west), frequent periods of high wind speeds and complex flow patterns characteristic of mountain climates (Barry, 1993) are observed. These site characteristics provide a rigorous challenge to eddy flux measurements, and paramount to validation of measured fluxes at this site is a critical evaluation of the energy budget. This study provides an assessment of the energy budget of a subalpine forest in complex terrain, discussing the extent that topographical complications can influence measurements of the energy budget components.

2. Site description

The study was conducted at the Niwot Ridge AmeriFlux site in the Roosevelt National Forest in the Rocky Mountains of Colorado (40°1′58.4″N and 105°32′47.0″W, 3050 m elevation). It lies approximately 25 km west of Boulder, Colorado and about 8 km east of the continental divide. A topographical map of the immediate area is shown in Fig. 1a. The site sits on a glacial moraine with an east–west slope of about 6–7°. To the west, forested fetch continues for nearly 2 km, while to the east of the tower, the fetch extends about for 300–400 m before the slope increases to ∼10–13° near the edge of the moraine.

The meteorology of this area has been well documented in previous studies (Barry, 1973; Brazel and Brazel, 1983; Parrish et al., 1990). Predominant winds are from the west, particularly in the winter months when there are frequent periods of high wind speeds that result in neutral atmospheric stability conditions. Summertime conditions are often typical of valley–mountain flow, with buoyancy driven upslope flow from the east occurring on many afternoons (∼30–40%). Night-time flow is typically katabatic (downslope drainage) flows from the west. Fig. 1b shows the sonic anemometer tilt angle in the u–w

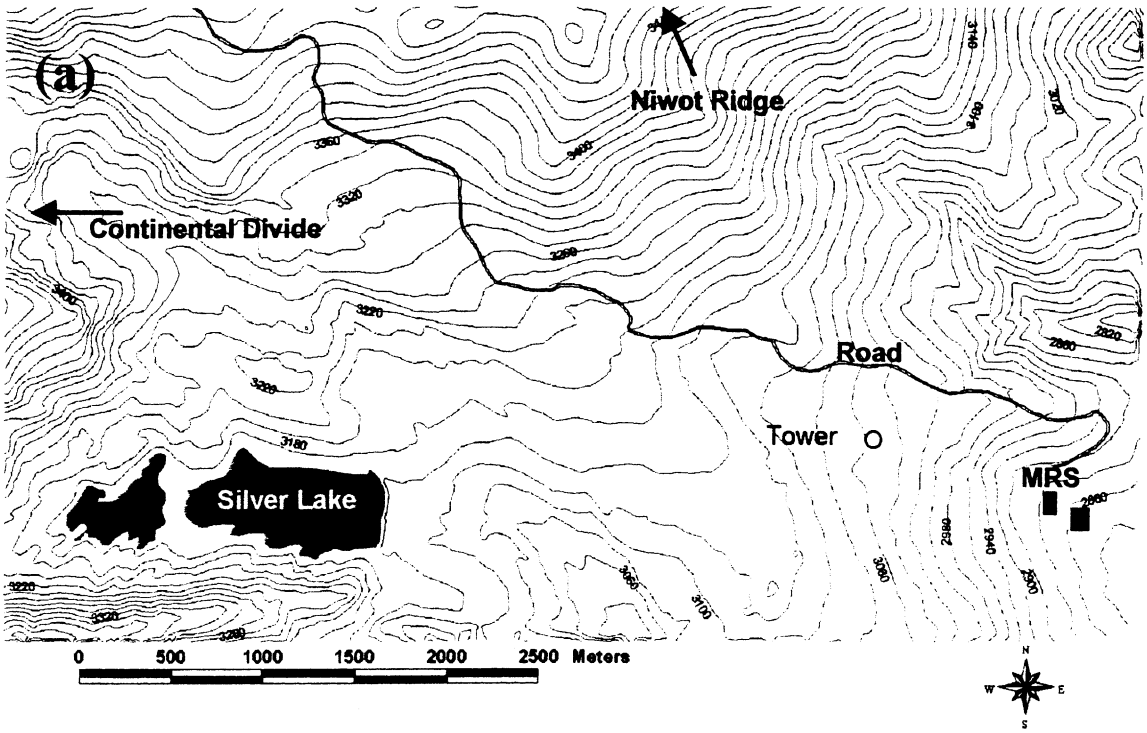

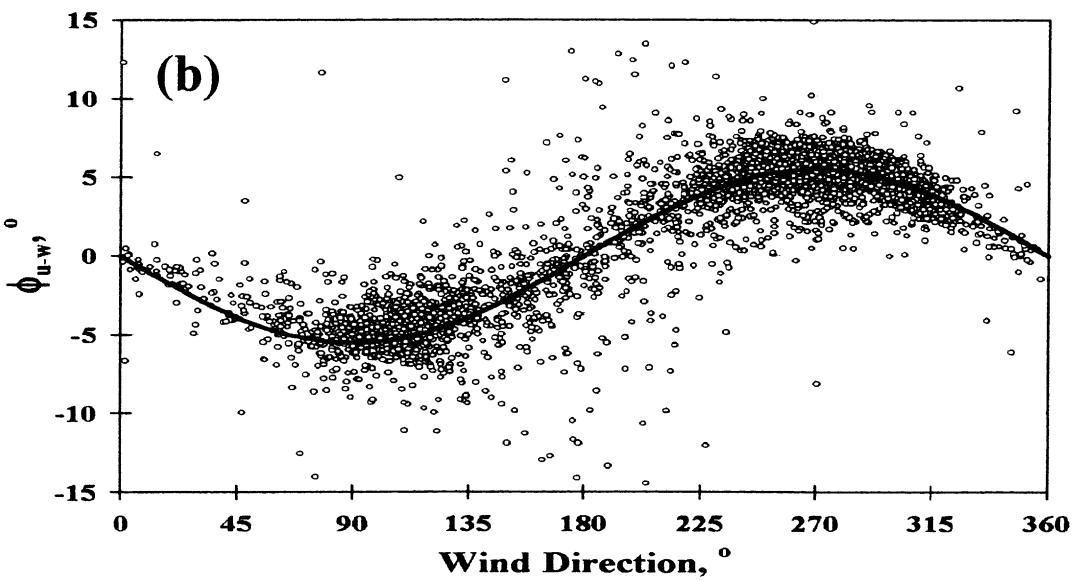

Fig. 1. (a) Topographic map showing the location of the tower. MRS: University of Colorado Mountain Research Station. The continental divide is ∼8 km west of the marked tower location. The road shown is a limited-access road which is traveled by approximately five vehicles per day in summer and is closed in winter. Contour labels are in meters and each contour represents 20 m. (b) Plot of the rotation transform angle in the u–w plane as a function of wind direction. Negative rotation angles are defined for flow coming up the slope. The line drawn is a fit to a fifth-order polynomial.

plane (described in Section 3) as a function of wind direction for June and July 2000. The two predominant wind directions are clearly discernible, centered around 105 and 270°. Upslope flows are much less common in the winter and are generally caused by synoptic storm systems passing to the south of the region as opposed to thermally-induced. Due to the distinct differences in meteorological conditions with season and wind direction, this paper will focus on contrasts between these often-encountered situations (winter–summer, upslope–downslope).

The site contains a mixed coniferous forest composed of subalpine fir (*Abies lasiocarpa*), Engelmann spruce (*Picea engelmannii*) and lodgepole pine (*Pinus contorta*). Table 1 includes some of the basic characteristics for this forest such as canopy height and leaf area index (LAI). The forest is approximately 90 years old, and was established following clear-cut logging. Very little understory is present due to the vertically dense canopy. The understory canopy consists of communities of wild blueberry (*Vaccinium myrtillus*), which grow close to the ground (height ∼10–15 cm, 25% average ground coverage). Soils are extremely rocky (granite) consisting primarily of mineral clays covered with a surface layer (∼10 cm) of organic material.

Table 1
Vegetation and canopy characteristics of the forest within 500 m of the measurement location

Canopy height (h_c)[a] (m)	11.5 ± 0.5
Displacement height (d)[b] (m)	7.6 ± 0.2
Roughness length (z_0)[b] (m)	1.79 ± 0.07
LAI[c] ($m^2\,m^{-2}$)	3.8–4.2
Canopy gap fraction[d] (%)	17 ± 3.5
Stand density (S_D)[e] (trees m^{-2})	0.40
Needle biomass (ρ_n)[f] (kg m^{-2})	3.79
Soil bulk density (ρ_s)[g] (g cm^{-3})	0.65 ± 0.10

Errors are S.E. ($\sigma/\sqrt{N}$) unless otherwise noted.

[a] Mean canopy height represents measurements from $N = 15$ sample plots.

[b] Displacement height and roughness length were determined from 314 vertical wind profiles under neutral stability.

[c] LAI was determined from harvesting of 15 trees (varying species and size), followed by scaling tree census data in a 1 km^2 area surrounding the tower.

[d] Canopy gap fraction represents data from six transacts.

[e] Determined from tree census data.

[f] Determined from tree harvesting. Value is for dry weight of needles.

[g] Density is the average of the top 10 cm of soil.

3. Materials and methods

3.1. Measurement of turbulent fluxes

Eddy covariance fluxes were measured at a height of 21.5 m ($z = 1.89h_c$, ∼10 m above the canopy) from a 26 m tall scaffolding tower. Wind speed and temperature fluctuations were measured with a three-dimensional sonic anemometer (CSAT-3, Campbell Scientific) mounted on a horizontal boom extending 1.8 m from the western edge of the tower. The boom was oriented at 204° to minimize shadowing from the tower for both downslope (westerly) and upslope (easterly) flow. A second triaxial sonic anemometer (ATI-K, Applied Technologies, Inc.) was used periodically at various heights as a second measure of both wind velocities and temperature.

Water vapor fluctuations were measured by two complementary methods. An open-path krypton (Kr) hygrometer (KH20, Campbell Scientific) was mounted approximately 36 cm to the east of the sonic anemometer. In the second (closed-path) water vapor measurement system, air was drawn from an inlet located 20 cm from the sonic anemometer sensing path and through an infrared gas analyzer (IRGA) (Model #6262, Li-Cor, Inc.), which was also used for measuring concentrations of CO_2. Air entering the inlet line passed through a stainless steel filter (2 μm) followed by 18 m of sampling tube (DeKabon 1300, Furon/DeKoron Division) with an inner diameter of 4 mm. To reduce temperature fluctuations, the sampled air then passed through 1.3 m of coiled copper tubing (4 mm i.d.) housed inside a weatherproof box with the gas analyzer. Airflow then passed through the analyzer and a mass flow meter before exiting the box. The flow through the analyzer was maintained at 8.5 L min^{-1} by a carbon-vane pump (Model #1351, Gast, Inc.) separated from the analyzer by a 4 L ballast to reduce pressure fluctuations. This flow rate was high enough to be turbulent flow (Reynolds number > 3000), reducing the loss of high frequency fluctuations caused by axial diffusion within the inlet tube (Leuning and King, 1992; Leuning and Judd, 1996). Pressure within the IRGA was 21 kPa below atmospheric pressure. The IRGA was operated in absolute mode with a constant slow flow of ultra-high purity (UHP) nitrogen passed through the reference cell. The reference gas was initially passed through

soda lime and magnesium perchlorate, removing trace amounts of CO_2 and H_2O. The system was automatically calibrated every 4 h by introducing reference gas, followed by a CO_2 span gas to the sample cell under the same temperature and pressure conditions as during sampling. Water vapor concentrations could not be automatically calibrated, and the span of the instrument was checked by comparing the H_2O mixing ratio measured by the IRGA to those calculated from relative humidity, temperature and pressure at the same height as the inlet. Typically these were within 10% and the IRGA readings were scaled accordingly.

Signals from the Campbell sonic anemometer, Kr hygrometer and IRGA were measured by a datalogger (CR23x, Campbell Scientific) at 10 Hz and then sent to a 486-PC. The raw (non-linear) outputs for CO_2, H_2O, temperature and pressure were recorded from the IRGA. The ATI sonic was directly connected to the 486-PC and its sampling rate varied from 10 to 20 Hz, depending on experimental exercise. The PC collected serial signals from several dataloggers, synchronized these signals in time and output these measurements via a fiber optic cable to a Sun workstation located in a trailer about 600 m away. Both the 486-PC and the Sun workstation used the ASTER software package developed in the Atmospheric Technology Division (ATD) at the National Center for Atmospheric Research (NCAR) for ingesting and archiving the raw data (Businger et al., 1990). The data was then transferred nightly via Ethernet to a second Sun workstation at the University of Colorado and subsequently backed up to a tape drive.

In general practice, the mean lateral ($\bar{v}$) and vertical ($\bar{w}$) wind velocities were mathematically rotated to zero following the procedure described by Kaimal and Finnigan (1994). A plot of the u–w transform angle (which forces $\bar{w} = 0$) versus wind direction is shown in Fig. 1b and indicates rotation angles of ±4–8°. This is in agreement with topographical inclinations shown in Fig. 1a. Turbulent fluxes were then derived from the covariance between the fluctuating components of vertical wind velocity (w') and the scalar of interest (x'):

$$F(x) = \overline{w'x'} = \overline{(w - \bar{w})(x - \bar{x})} \quad (1)$$

where primes denote fluctuations from the mean and overbars denote mean values. Means and fluxes were typically calculated as a block average over a 30 min time period. Sensible heat fluxes (H) were derived from the covariance between temperature (T') and vertical wind velocity, $H = c_{pm}\rho_a\overline{w'T'}$, where ρ_a is atmospheric density and c_{pm} is the heat capacity of moist air (Webb et al., 1980). Temperature was measured from the sonic virtual temperature (T_v) corrected for wind speed normal to the sonic path (on-line by both sonic anemometers) and humidity (Schotanus et al., 1983). A comparison of sensible heat fluxes from the two sonic anemometers is shown in Fig. 2a where both anemometers were mounted at similar heights. As seen in the figure, heat fluxes calculated from the two sonics agreed to within 5%.

Latent heat fluxes (λE) from both the open- and closed-path systems were calculated from the observed covariances between water vapor density (q) and vertical wind velocity, multiplied by the temperature-adjusted latent heat of vaporization, L_v. Fluxes from the open-path Kr hygrometer were corrected for oxygen absorption and for density fluctuations due to sensible heat according to Webb et al. (1980). No sensible heat correction was necessary on the closed-path system since the gas was brought to a common temperature before analysis (Leuning and Judd, 1996). Lag times between sensors were calculated by maximizing the cross correlation between the respective scalar signal and the w wind velocity. The Kr hygrometer showed little or no lag with respect to both w and sonic temperature, T_v. The effect of applying this lag to λE was small (<2%) and, therefore, neglected. The closed-path system created a lag of ~1.7 s for H_2O vapor measurement (depending on the exact flow rate), and the H_2O time series was shifted forward in time by this amount relative to w before the covariances were calculated. Fig. 2b shows the agreement between the two methods of calculating latent heat flux. Overall the closed-path system tended to underestimate λE by ~3–7% relative to the open-path Kr hygrometer. This was most likely due to loss of high frequency (>1 Hz) fluctuations which are damped out by both the flow through the inlet tubing and electronic processing in the IRGA.

The only times when the instruments did not exhibit good agreement occurred after significant snowfall. During these anomalous periods, the closed-path system would underestimate λE by as much as 50% relative to the Kr hygrometer. Concurrent at these times, a

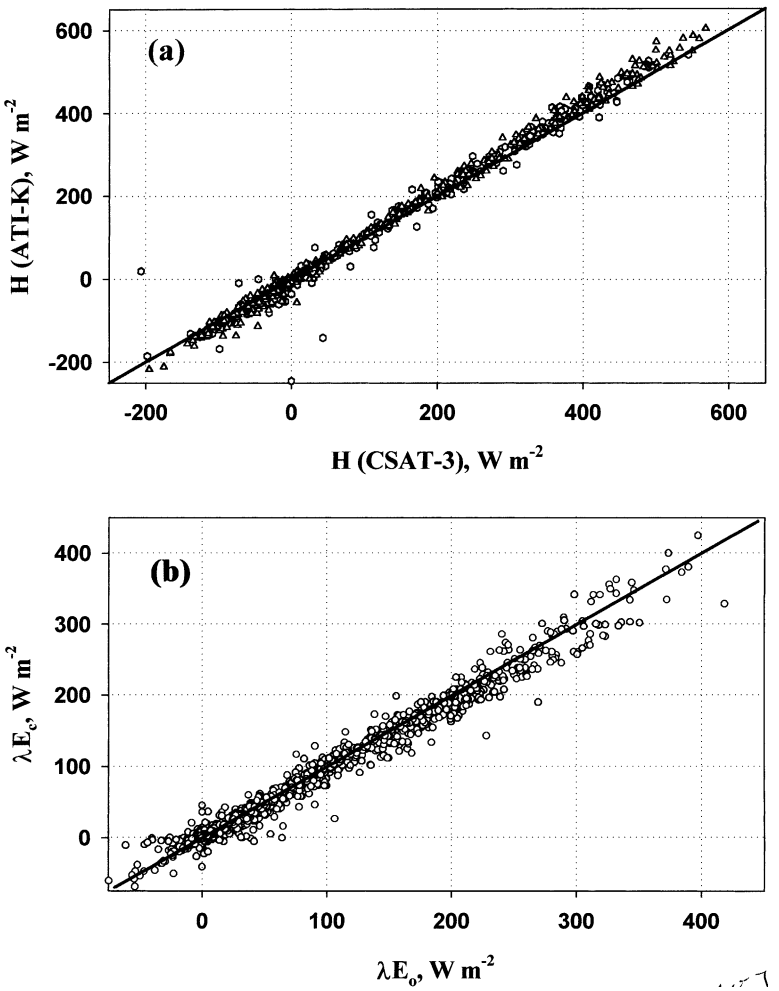

Fig. 2. (a) Plots of H measured by the CSAT-3 sonic anemometer compared to those from the ATI-K sonic. Symbols are: ○, time period of 15 May–5 June 1999, both sonics operated at 10 Hz; △, time period of 15 March–10 April 2000, ATI-K sonic sampled at 20 Hz, CSAT-3 sampled at 10 Hz. (b) Comparison of latent heat fluxes determined from the open-path Kr hygrometer (λE_o) and the closed-path IRGA (λE_c). Measurements were compiled from 10 days periods in June and September 1999, March, June, August and November, 2000. Lines drawn in both plots are the 1:1 line. Linear regression slopes are 1.04 and 0.95 for (a) and (b), respectively.

significant lengthening of the lag time was observed, even though the flow rate remained unchanged. We attribute these effects to condensation of water vapor at the inlet of the closed-path system, leading to prolonged absorption and revolatilization of H_2O. This condition generally corrected itself after about 1–2 days or could be manually corrected by changing the inlet filter. At these times, only fluxes from the open-path Kr hygrometer were considered valid and used for analysis.

3.2. Supporting meteorological and energy balance measurements

Along with the turbulent flux measurements described above, a variety of radiation, meteorological and biometric measurements were undertaken. Temperature and relative humidity sensors (Model HMP-35D, Vaisala, Inc.) were mounted in ventilated mounts (Model 43408-2, RM Young, Inc.) at $z = 2$, 8, and 21.5 m. Barometric pressure was measured

using a capacitance manometer (Model PT101B, Vaisala, Inc.) at $z = 18$ m. Wind speed and direction were also measured at $z = 26$ m and (in year 2000) 16 m by two propvane anemometers (Model 09101, RM Young, Inc.) mounted on 2 m booms extending from the north side of the tower. Radiation measurements were made at $z = 26$ m using a net radiometer (Model Q*7.1, REBs), a four-component net radiometer (Model CNR-1, Kipp and Zonen) and two quantum sensors (Model Li190-SA, Li-Cor, Inc.) facing upwards and downwards. The radiometers were mounted on 2 m booms directed at 204°, whereas the quantum sensors were mounted on a 1 m boom facing 114°. The Q*7.1 radiometer was ventilated (Model RV-2, REBs) and wind corrections were applied accordingly. No shadowing from the tower or other sensors was evident in the diurnal profiles from these sensors. The two radiometers were compared at various times between August 1999 and March 2001 indicated agreement within 4% for typical day-time values of the mean net radiation (R_{net}). The regression slope of the comparisons remained constant over the entire 18 months period (1.02 ± 0.02), suggesting that the two instrument calibrations remained fairly constant. Night-time measurements of net radiation showed substantial discrepancies between the two radiometers with a regression slope of 1.25 (using the REBs radiometer as the independent variable). This indicated an error in the 'long-wavelength measurement of one or both radiometers (this will be discussed further in subsequent sections).

A further comparison to illustrate the stability of the radiometer calibration consisted of comparing the incoming short wave radiation (from the CNR-1) and incoming photosynthetically active radiation (PAR, Li-SA90) between July 1999 and September 2000. Linear regressions were calculated every 10 days and the slopes of these regressions varied less than 2% over the entire time period. Outgoing short wave radiation was also compared with outgoing PAR in the same manner and varied less than 10%. The larger error in this comparison is attributed to the smaller intensities of the measured reflected light, leading to smaller signals. There was, however, no indication of a trend in the comparisons, which might indicate a shift in calibration.

Soil heat flux (G) was determined from ten soil heat flux plates (Model HFT-1, REBS) distributed in pairs and buried at 7–10 cm below the surface in a variety of microenvironments (ranging from mostly sunlit to mostly shaded). Heat storage in the soil above the plates (S_s) was not routinely measured due to a lack of continuous soil moisture measurements. However, continuous soil temperature measurements (T_s, model STP-1, REBS) were used in conjunction with periodic measurements of average volumetric soil moisture and the soil bulk density to estimate S_s. This showed that the heat storage in the upper soil layers was small (<1–2% of R_{net}) and was neglected.

Heat storage in the boles (S_b) was calculated via

$$S_b = \frac{S_D \rho_b c_{pb}}{n} \sum_{i=1}^{n} V_{bi} \frac{\Delta T_{bi}}{\Delta t} \quad (2)$$

where S_D is the stand density (0.40 stem m^{-2}), ρ_b the average bole density (kg m^{-3}, measured from a series of 35 tree cores), c_{pb} the average bole specific heat (kJ kg^{-1} K^{-1}) and Δt is the sampling period (1800 s). V_{bi} and T_{bi} were taken from sampled trees ($n = 8$) across the three dominant species (two lodgepole pines, three subalpine fir and three engelmann spruce). T_{bi} is the bole temperature measured from a series of 16 thermocouples (Model #107-L, Campbell Scientific) imbedded at depths of 2 and 8 cm. V_{bi} is the estimated bole volume obtained from a relationship derived from measuring the bole diameter at breast height (DBH). The relationship between DBH and bole volume was deduced from the harvesting of 15 trees (from all species and size classes) in which the bole volume was explicitly measured (Monson et al., 2001). The bole specific heat was calculated from $c_{pb} = (c_D + W_b c_w)/(1 + W_b)$ (Marshall, 1958), where W_b is the average water content on a dry mass basis, c_D the specific heat of dry wood (1.37 kJ kg^{-1} °C^{-1}, Dunlap, 1912), c_w is the specific heat of water (4.19 kJ kg^{-1} °C^{-1}). Water content in the boles (W_b) was measured gravimetrically from a series of 35 tree cores sampled across the various species. Cores were taken in late summer ($W_b = 45\%$) and in the late fall ($W_b = 35\%$) after photosynthesis had ceased.

Energy storage in the needles was calculated from

$$S_n = \frac{\rho_n c_n}{(1 - W_n)} \frac{\Delta T_n}{\Delta t} \quad (3)$$

where W_n is the gravimetric water content of the needles (~55%), ρ_n the average needle density (3.79 kg

needle m^{-2} land area, on a dry mass basis), c_n the specific heat of the needles, and Δt is the sampling period (1800 s). Needle specific heat was obtained from $c_n = 0.55c_w + 0.45c_c$, where c_c is the specific heat of cellulose (Ganster and Fink, 1999). Needle temperature (T_n) was estimated using the air temperature measured within the canopy at a height of 8 m and assuming that changes in needle temperature would be reflected in the air temperature. This was valid since the small leaves and windy conditions typical of our site leads to formation of a thin laminar sub-layer at the needle surface, and, thus, tighter coupling between air and needle temperature (Oke, 1987).

Storage fluxes of H and λE within the airspace beneath the height of the turbulent flux measurement were obtained from profiles of temperature and relative humidity at 2, 8 and 21.5 m. The storage terms were then calculated from

$$S_H + S_{\lambda E} = \rho_a c_{pm} \int_0^z \frac{dT}{dt}\, dz + \frac{\rho_a c_{pm}}{\gamma} \int_0^z \frac{dq}{dt}\, dz \quad (4)$$

where γ is the psychometric constant (4×10^{-4} $g_{water}\, g_{air}^{-1}\, K^{-1}$) and dT/dt and dq/dt are the changes in the either the air temperature (T) or water vapor density (q) over the 30 min time period.

Energy consumed in the process of photosynthesis (J_a) was calculated from fluxes of day-time net ecosystem exchange (NEE measurements described in Monson et al. (2001)) using the photosynthetic energy conversion factor ($0.469\, J\, \mu mol^{-1}$) (Blanken et al., 1997). This led to small underestimations of this energy term since the respiration component of NEE was not subtracted out. However, J_a typically was <1% of the average daily net radiation, therefore, this had little effect on the overall energy budget.

4. Results

4.1. Evaluation of turbulent flux quality

All of the 30 min time series of w, T_v and q were initially checked to be sure that means and variances were within reasonable ranges and to eliminate any anomalous spikes within the data caused by instrumentation malfunction or external sources (e.g. precipitation). Data sets were tested for stationarity and integral turbulence statistics using the method described by Foken and Wichura (1996). These two tests typically eliminated ~17% of the data (on a monthly basis). The effects of co-ordinate rotation on the measured fluxes will be discussed in a subsequent paper. Footprint analysis using the model of Schuepp et al. (1990) implied adequate fetch under most circumstances, the exception being during higher wind speeds from the east, which were infrequent.

It is well established that frequency-based corrections to flux measurements are necessary in many situations (Moore, 1986; Massman, 2000). The most commonly employed corrections are high-pass filtering by either linear detrending or block averaging and corrections for effective low-pass filtering due to sensor separation, response time, or flow through an inlet tube prior to analysis. Calculation of the co-spectral transfer function for block averaging (Massman, 2000) using our standard averaging period of 30 min indicated that corrections to the low frequency end of the spectrum were negligible. In general, the time series of wind velocity, temperature and water vapor (both systems) were not detrended. This decision was made following work on subsets of data which were linearly detrended before calculating the covariances (fluxes) and compared to the non-detrended fluxes. For both winter and summer data (~1 month of each), regressions of non-detrended versus detrended fluxes were highly linear with slopes ranging from 0.97 to 1 ($R^2 =$ 0.90–0.98).

High frequency flux loss can have several origins (Moore, 1986; Leuning and Judd, 1996; Massman, 2000). Line/volume averaging, sensor separation, and attenuation due to tubing are all forms of low-pass filtering. Evaluating their possible effects requires analysis of the observed power spectra for single components and the one-sided co-spectrum for covariances. Fig. 3 shows average power spectra for T and q (both systems) and co-spectra for $w'T'$ and $w'q'$ obtained under typical day-time conditions during summer. As can be seen, all power spectra indicated the inertial subrange at $f > 0.08$ Hz up to near the Nyquist frequency ($f = 5$ Hz). Some aliasing of higher frequency contributions was observed between ~2 and 5 Hz in the CSAT-3 sonic anemometer whereas no aliasing was evident for the ATI-K. This is because the CSAT-3 was sampled at 10 Hz (without oversampling) whereas the ATI-K is oversampled at 200 Hz and then block-averaged back to 10 (or 20) Hz. The

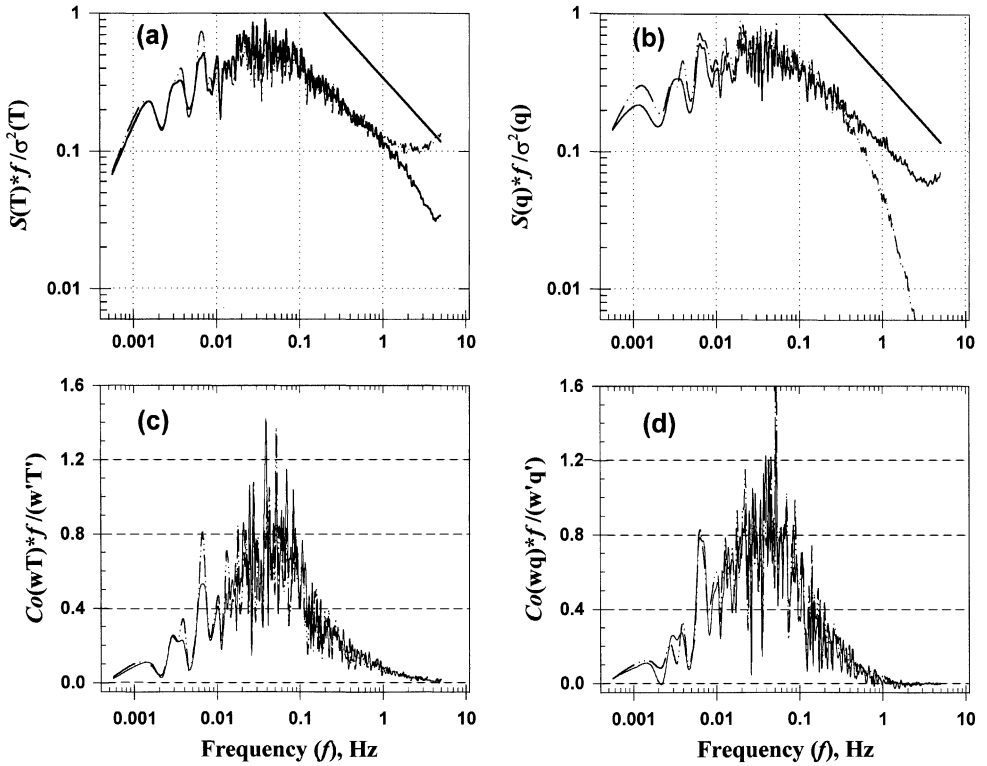

Fig. 3. (a) Virtual temperature power spectrum averaged over 14, 30 min periods, on a "typical" day, 28 May 1999, $U \sim 4\,\mathrm{m\,s^{-1}}$, $u^* \sim 0.4$–$0.7\,\mathrm{m\,s^{-1}}$. Solid line: ATI-K sonic; dot–dash line: CSAT-3 sonic. (b) Water vapor (q) power spectrum over the same time period. Solid line: Kr hygrometer; dot–dash line: IRGA system. Spectra in (a) and (b) are multiplied by frequency and normalized by the variance of the scalar. The solid straight line on both plots indicates the expected $-(2/3)$ slope. (c) Co-spectra of $w'T'$ obtained under the same conditions as (a). (d) Co-spectra of $w'q'$ during the same period. Solid line and dot–dash line descriptions in (c) and (d) are identical to (a) and (b), respectively. Co-spectra are multiplied by frequency and normalized by the co-variance.

oversampling of the ATI-K anemometer acts as a filter to remove high frequency aliasing (Kaimal and Finnigan, 1994). However, as seen in the $w'T'$ co-spectra, the area beneath the curves for the ATI and the CSAT-3 are nearly identical, as there is little contribution to the flux above 1 Hz (<2.5%). This is further verified by Fig. 2a, where sensible heat fluxes from both sonic anemometers were in excellent agreement, regardless of sampling mode.

Co-spectral transfer functions have been developed to correct measured fluxes for errors due to line averaging, sensor separation, etc. (see Massman, 2000 for compilation). To evaluate the possible significance of each of these errors, effective time constants (given in Massman, 2000) can be calculated. Time constants for line averaging were typically greater than 10 Hz for all measurements, thus, these corrections were neglected. Sensor separation arises from the physical displacement of one sensor from the volume where the wind velocity is measured, and can contribute to losses of water vapor flux in both systems. The lateral translation distance between the sonic path and the Kr hygrometer was ~36 and ~20 cm to the inlet to the IRGA system. During moderately unstable periods ($U \sim 4\,\mathrm{m\,s^{-1}}$, $(z-d)/L \sim -0.3$), the cut-off frequency (f_{co}, defined as the frequency at which the co-spectral transfer function equals 0.7) for sensor separation are $f_{co} \sim 7.3$ and 11 Hz for the Kr hygrometer and IRGA, respectively. In general, this is more significant at night during low wind speeds ($f_{co} \sim 2.4$ Hz for Kr hygrometer with $U = 1\,\mathrm{m\,s^{-1}}$). Using the transfer function of Moore (1986), it was found

that sensor separation caused at most a 2% loss of flux at the high frequency end of the co-spectrum for the Kr hygrometer during day-time conditions. It is difficult to get a reliable estimate of the error at night, since latent heat fluxes were small ($<40\,W\,m^{-2}$) and the co-spectra was noisy during these periods. Since the inlet to the IRGA systems was closer to the sonic than the Kr hygrometer, the correction for sensor separation was even less relevant.

The passage of the sampled air through the inlet tubing of the closed-path system can also act to dampen high frequency fluctuations. With typical values for the Reynold's number, gas velocity and tubing dimensions ($Re = 3085$, $v = 11.3\,m\,s^{-1}$, $r = 0.002\,m$, $L = 18\,m$), the corresponding cut-off frequency is estimated to be $f_{co} \sim 2.3\,Hz$ (Leuning and Judd, 1996). Using the co-spectral transfer function for turbulent flow described by Lenshow and Raupach (1991), underestimation of the flux for H_2O vapor (and CO_2) from the closed-path system was less than 2% during most of the summertime situations. However, by looking at Fig. 3b, it is apparent that the closed-path system tends to lose spectral power at lower frequencies ($f > 0.6\,Hz$) than the calculated cut-off frequency. This is likely due to the presence of filters along the flow path and the larger sampling volume within the IRGA detection cell. Although these lower the effective cut-off frequency of the closed-path system, the direct comparison between the open- and closed-path sensors (Fig. 2b) indicates that this only reduces the measured latent heat fluxes by ~3–7%. Tubing attenuation becomes an increasingly important factor in flux loss during periods where atmospheric stability causes co-spectral intensities to shift towards higher frequencies. However, these conditions are usually encountered either at night (stable conditions) or during winter (high wind speeds, neutral stability) when latent heat fluxes tend to be small (<20–$60\,W\,m^{-2}$). Therefore, even 10–15% corrections to the high frequency end of the $w'q'$ co-spectrum make little difference in the overall energy budget.

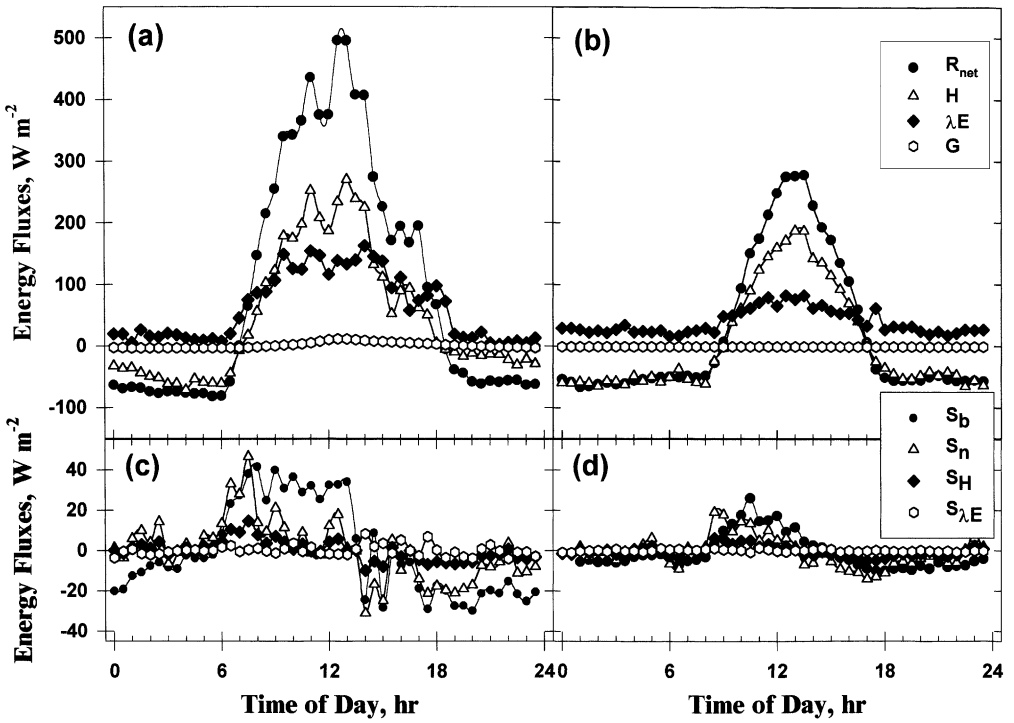

Fig. 4. (a) Ten days average of energy fluxes (R_{net}: net radiation, H: sensible heat, λE: latent heat, G: soil heat flux) for 11–20 August 2000. (b) 10 days average of energy fluxes for 11–20 January 2000. (c) Average storage fluxes (S_b: bole, S_n: needle, S_H: sensible heat and $S_{\lambda E}$: latent heat) from 11 to 20 August 2000. (d) Storage fluxes averaged over 11–20 January 2000.

4.2. Energy balance measurements

The energy budget at a given site is defined as

$$R_a = R_{net} - G - S_T = H + \lambda E \quad (5)$$

where R_a is the available energy, typically defined as the net radiation (R_{net}) minus the soil heat flux (G) and storage terms (S_T). S_T can be partitioned according to

$$S_T = S_H + S_{\lambda E} + S_b + S_n + J_A \quad (6)$$

where S_H and $S_{\lambda E}$ are defined as the storage of sensible and latent heat within the air space below the measurement height, S_b is heat storage within the boles, S_n is heat storage within the canopy needles and J_A the energy used in photosynthesis. Fig. 4 shows typical 10 days average diurnal trends of these fluxes for both summer and winter. As shown in the figure, soil heat flux (G) and heat storage (S_T) typically account for 8% (or less) of R_{net}. In general, sensible heat was the largest component of the energy budget as indicated

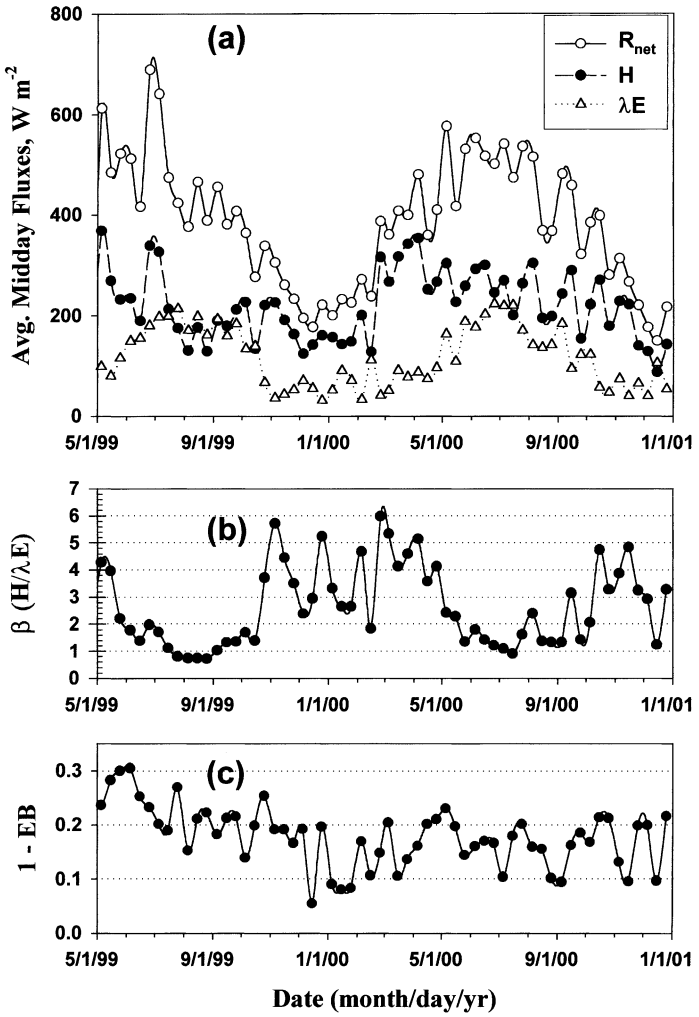

Fig. 5. Seasonal variation of mid-day energy fluxes from May to December 1999: (a) 10 day averages of R_{net}, H and λE during mid-day (10:00–14:00, local time); (b) mid-day average Bowen ratios (β); (c) energy budget residual (1 − EB). EB was obtained from a linear regression of ($H + \lambda E$) vs. R_a for each 10 day period. Note that higher residuals before July 1999 are due to the lack of incorporating the storage flux terms which were not measured at this time.

by Bowen ratios ($\beta = H/\lambda E > 1$) during most day-time periods. This is illustrated in Fig. 5a which shows the average (10 days) mid-day energy fluxes (R_{net}, H and λE) over the time period from May 1999 through December 2000. Exceptions to this generality occurred during a few short days in late spring and during a very rainy period in August 1999 which lasted most of the month. At these times Bowen ratios reached minimum values ranging between 0.7 and 0.9 (Fig. 5b).

Fig. 6 shows plots of ($H + \lambda E$) versus R_a for both summer and winter day-time periods. It excludes data where turbulent mixing was considered inadequate or temperature fluctuations were unmeasurable. A discussion of these periods is given subsequently. Linear regressions of all the data yielded slopes of 0.84 ± 0.02 ($R^2 = 0.92$) and 0.88 ± 0.01 ($R^2 = 0.94$) for summer and winter, respectively. The error reported is the S.E. ($\sigma/\sqrt{N}$) of the slopes of these plots only, they do not include any estimation of systematic error. This analysis suggests that we can account for >80% of the available energy on a half-hourly basis. The energy budget was also studied during transition seasons (spring and fall). In general, there was slightly less

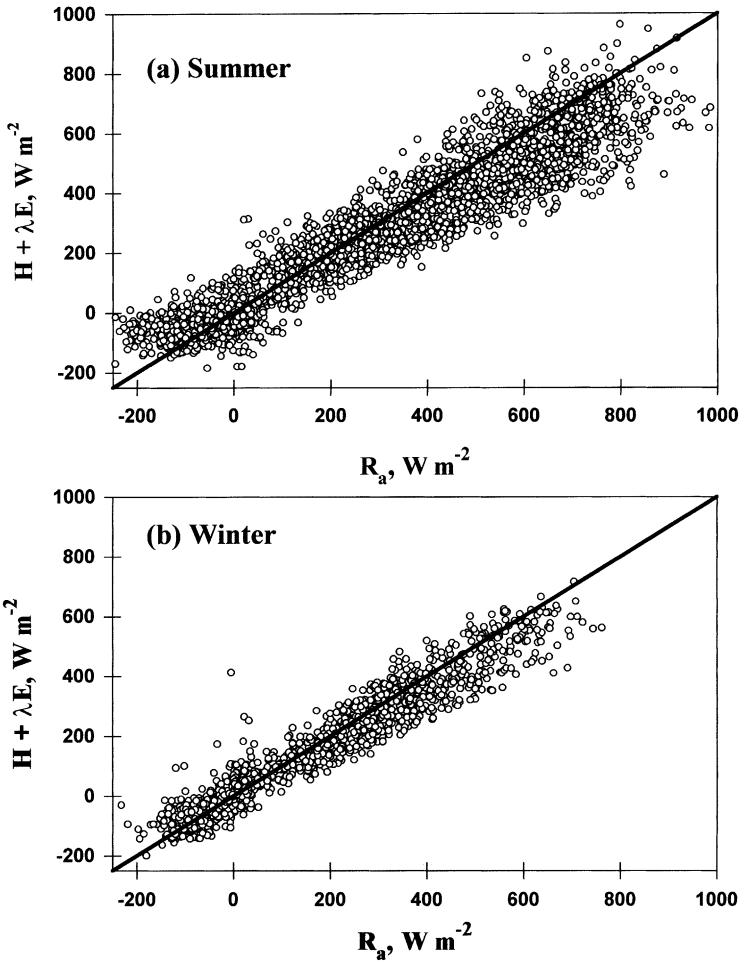

Fig. 6. Plots of sensible + latent heat flux ($H + \lambda E$) vs. available energy ($R_a \equiv R_{net} - G - S_T$). The solid line represents the 1:1 line. Time periods are: (a) summer (includes data from July–September 1999 and June–September 2000); (b) winter (includes data from December 1999–March 2000). Linear fits to the data yielded slopes of 0.84 and 0.88 and intercepts of 7.3 and 3.3 $W m^{-2}$ for summer and winter, respectively.

success in closure during these seasons (0.81 ± 0.02 during spring and 0.82 ± 0.02 during fall). This can be seen as peaks in the energy budget residual shown in Fig. 5c. Springtime also shows a radical change in mid-day Bowen ratio (see Fig. 5b), decreasing from values between 4 and 6 in March down to near unity in mid-May–June. An opposite trend in the Bowen ratio is observed in the fall as evapotranspiration slowed and sensible heat again became dominant.

Closure of the energy budget was slightly better under conditions of downslope winds, obtaining slopes of 0.88 ± 0.02 and 0.89 ± 0.01 for linear regressions of $H + \lambda E$ versus R_a for wind directions between 220 and 320° (summer and winter, respectively). This is compared to closure of 0.80 ± 0.02 and 0.75 ± 0.05 over the same time periods for wind directions between 60 and 160°. This directional bias in budget closure was also apparent during the spring and fall data as well.

Direct comparisons between the CNR-1 and the REBs Q*7.1 radiometers at night (when only the long-wave component of net radiation is important) indicated a significant discrepancy. Measurements from the CNR-1 were about 25% larger (more negative) than corresponding measurements using the

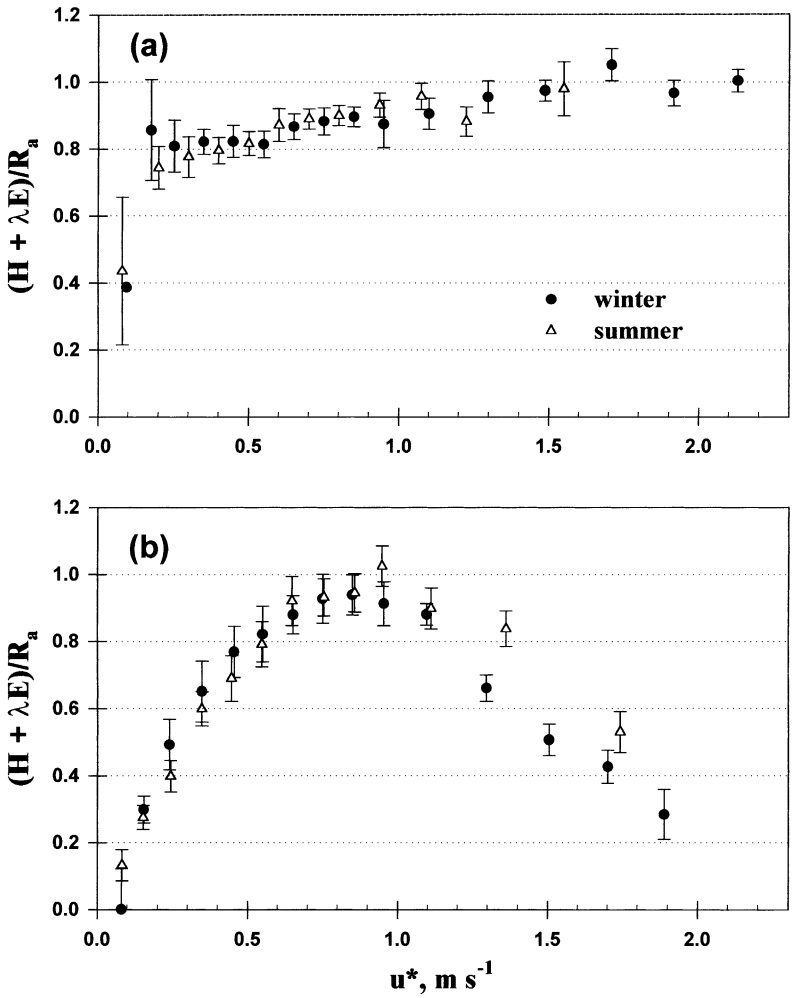

Fig. 7. Plots of the energy balance ($(H + \lambda E)/R_a$) vs. friction velocity (u^*) for both (a) day-time ($R_a > 30\,W\,m^{-2}$) and (b) night-time ($R_a < -30\,W\,m^{-2}$) conditions. Data are binned in intervals of $0.1u^*$ for $u^* \leq 1$ and $0.15u^*$ for $u^* > 1$. Error bars represent the S.E. ($\sigma/\sqrt{N}$, with N being the number of measurements in each bin).

REBs Q*7.1. There is no reason to believe that either is without some error; however, by looking at the night-time energy balance under well-mixed conditions, it was observed that use of the CNR-1 radiation measurements led to large energy deficits. Energy balance measurements using net radiation derived from the REBs radiometer were in reasonable agreement with day-time values under these suitable meteorological conditions. Therefore, we used the REBs radiometer measurements during periods when the long-wave radiation dominated and used a regression of nocturnal net radiation measurements to correct the long-wave component of the CNR-1 radiometer. However, further testing is advised to determine the source of this discrepancy.

Both night-time and day-time closure of the energy budget was affected by the local turbulence intensity. Fig. 7 shows a plot of $(H + \lambda E)/R_a$ versus friction velocity ($u^* = ((u'w')^2 + (v'w')^2)^{0.25}$, Stull, 1988) for both day and night. As can be seen, there were significant shortfalls in the closure of the energy balance at low u^* values, even during day-time conditions (although there are rather few data points under these conditions). Day-time low u^* periods tended to occur in early mornings and evenings during transitions between unstable and stable stratification. For the day-time conditions, energy budget closure attained values ~0.8 at u^* values >0.2 m s^{-1} and gradually approached full closure as u^* increased. At night, a peaked behavior was observed. Energy balance did

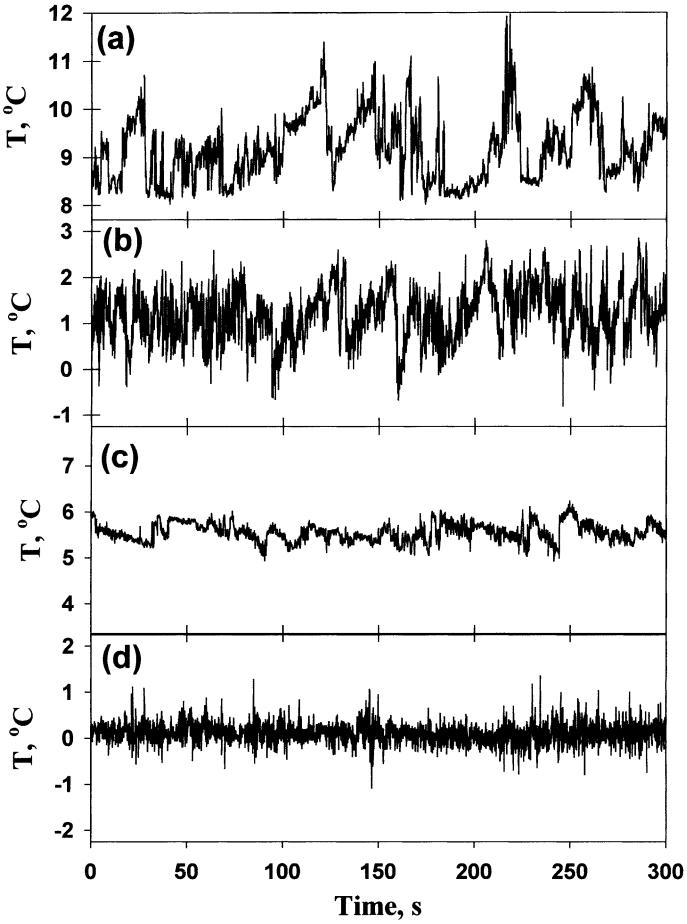

Fig. 8. Time series of the sonic temperature for four 5 min intervals under varying wind and radiation conditions: (a) 28 May 1999, 12:00 MDT, $u^* = 0.8\,\mathrm{m\,s^{-1}}$; (b) 19 March 2000, 12:00 MST, $u^* = 2.1\,\mathrm{m\,s^{-1}}$; (c) 4 June 1999, 4:00 MDT, $u^* = 0.25\,\mathrm{m\,s^{-1}}$; (d) 23 March 2000, 23:00 MST, $u^* = 2.0\,\mathrm{m\,s^{-1}}$.

not approach 0.8 until u^* values of $0.5\,m\,s^{-1}$ were measured and nearly full closure was attained at $u^* \sim 1\,m\,s^{-1}$. However, there was a significant decrease in the observed energy balance at high values of u^* ($>1.2\,m\,s^{-1}$) at night, regardless of season.

The reason for this loss of energy at high u^* lies in the resolution of the temperature measured by the sonic anemometer (regardless of brand) when temperature fluctuations are small. Since, latent heat exchange was typically close to zero at night (especially in winter), the majority of the turbulent exchange is in the form of sensible heat. Nocturnal sensible heat fluxes were considerably smaller relative to day-time values, as temperature gradients (and subsequently fluctuations) were much smaller. Increased turbulent mixing (occurring at high u^*) decreases the observed gradients further and can reduce the magnitude of the temperature fluctuations observed by the sonic anemometer towards the instrument's resolution limit.

Fig. 8 shows several 5 min time series of sonic virtual temperature measurements during periods of moderate and high turbulence ($u^* = 0.6$ and $2\,m\,s^{-1}$)

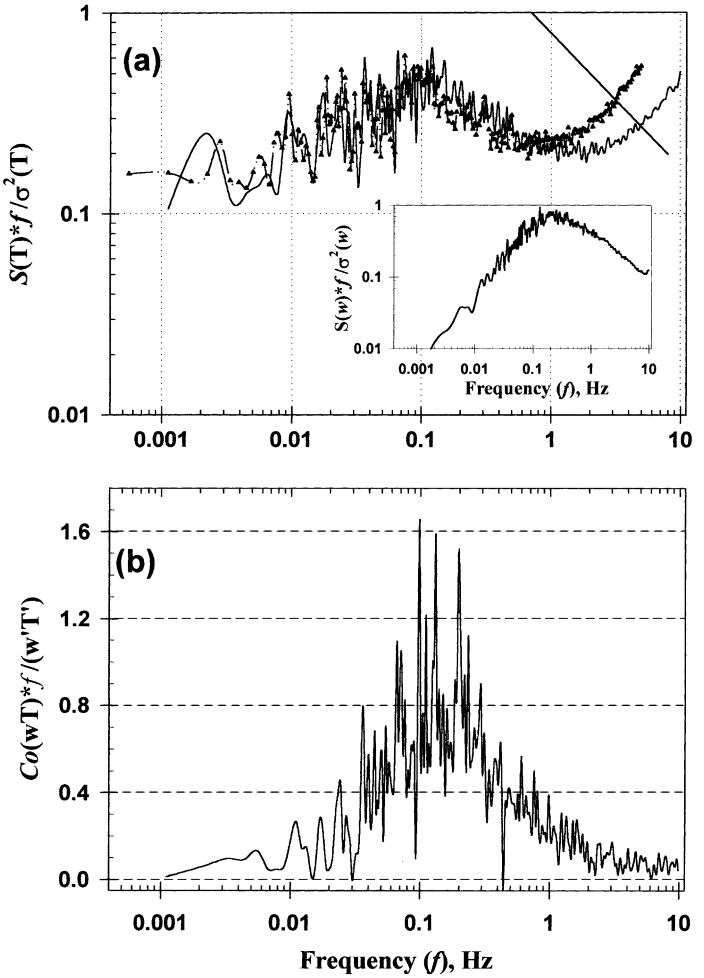

Fig. 9. (a) Power spectra of sonic temperature (solid line: ATI-K, 20 Hz sample rate; dashed line with points: CSAT-3, 10 Hz sample rate) during the day of 19 March 2000 under high turbulence event (average $u^* = 2.1\,m\,s^{-1}$ over 14, 30 min time periods). The inset shows the power spectrum for vertical wind velocity (w) during this period (from the ATI-K sonic). (b) Co-spectrum for $w'T'$ during the same time period—taken from the ATI-K. Co-variances from the CSAT-3 were in good agreement with that of the ATI-K (within 4%) over the entire time period and are included in Fig. 2.

during both day and night. Large buoyancy-driven temperature fluctuations are apparent as slower upward ramps followed by fast downward decays in day-time measurements, even under high turbulence. However, there is considerable distortion in the temperature time series at the higher u^* values. This becomes more evident in the night-time temperature traces. The small fluctuations observed in Fig. 8c under stable conditions are nearly completely obscured by this distortion at higher turbulence intensity (Fig. 8d). During these periods of large nocturnal u^*, the measured covariances between w and T approached zero, causing large shortfalls in the energy budget.

The occurrence of this noise and its effects on the day-time fluxes were examined by looking at the power spectrum of w and T and the $w'T'$ co-spectrum (Fig. 9). At frequencies above about 1 Hz, noise begins to dominate the temperature power spectra obtained from either sonic anemometer. The lack of noise in the w power spectrum (see Fig. 9a inset) or in the u and v power spectra (data not shown) argues against this noise being produced by vibrations in the tower or booms, or from deformation of the sonic heads in the high winds. As seen in the co-spectrum (Fig. 9b), the majority of the day-time flux contribution lies below the range where the noise dominated the spectrum, peaking at about 0.1–0.2 Hz. Only about 10% of the heat flux originated from frequencies greater than 1 Hz. This was similar to the high frequency flux contributions observed in the $u'w'$ co-spectrum (data not shown), which was not affected by noise. Assuming similarity between momentum and temperature fluxes, this suggests that the increased spectral intensity observed in the T spectrum due to the high frequency noise did not lead to an overestimate of the flux. Further support for this contention is the nocturnal H fluxes approached zero during high u^* periods, suggesting that the noise observed does not correlate with w and, therefore, does not contribute to the calculated covariances.

5. Discussion

5.1. Components of the energy balance and seasonal trends

Sensible heat was the dominant form of energy loss from the forest to the atmosphere during most time periods (Figs. 4 and 5). This is not unexpected based on results from other coniferous forests growing in harsh environments (Jarvis et al., 1976, 1997; Lindroth, 1985; Kelliher et al., 1993; Fitzjarrald and Moore, 1994; Laubach et al., 1994; Baldocchi et al., 1997). The latent heat flux at our site was typically tied to forest productivity and precipitation events. This flux generally increased in spring and summer (as carbon uptake increased), and decreased to smaller values during fall and winter as water became frozen. Latent heat fluxes in the winter were often low ($<50\,\mathrm{W\,m^{-2}}$), except immediately following snow events. This is illustrated in Fig. 5b where significant snowfall during the middle of February 2000, led to significantly larger average λE fluxes.

Seasonally, the Bowen ratio reached a maximum (>4) in early spring just prior to activation of net carbon uptake by the forest (Fig. 5b). Even though temperatures began to warm during this period, soils remained frozen under the snowpack. The lack of liquid water prevented transpiration. The large sensible heat fluxes and long-wave radiation originating from the canopy foliage during this period played an important role in increasing the temperature (and, thus, the condition) of the snowpack (Oke, 1987). When the snowpack becomes isothermal at 0 °C, liquid water can be moved from the surface downward into the soils. At this point, water becomes available to tree roots, transpiration is initiated and β begins to decrease.

Although mid-day Bowen ratios typically exceeded unity, we did observe periods when λE became greater or equivalent to H, leading to values of $\beta \leq 1$. One period occurred during the mid- to late-spring snowmelt, in contrast to the early spring when Bowen ratios were highest (Fig. 5). At the time of snowmelt, water availability was non-limiting and the trees were near their optimum temperature for carbon uptake (Monson et al., 2001), thereby, resulting in lower β values. The only other period we observed $\beta \leq 1$ was during August 1999 (see Fig. 5). At this time, the transport of moisture from the Gulf of Mexico along the western edge of a strong high pressure ridge situated in the middle of the continent (colloquially called "monsoonal flow") lead to relatively high humidities and enhanced upslope flow (or more precisely, reduced downslope flow which allows for upslope flow to develop) along the Colorado Front Range. The

flow of warm, humid air up the eastern flanks of the mountains led to the near-daily build-up of convective storms. Frequent rains during August 1999 led to near saturation of soils (volumetric soil water content, $\theta_w \sim 0.4\,m^3\,m^{-3}$) and the high degree of water availability to the vegetation likely led to the observed large latent heat fluxes. As this weather pattern subsided in September, β again increased to values >1.5 as soil water content decreased to values less than $0.2\,m^3\,m^{-3}$.

In contrast to 1999, monsoon flow was cut-off from Colorado during August 2000. This led to a significant drought beginning in late July and lasting into mid-August. Mid-day $\beta \sim 1$ were observed in mid-July, but then increased dramatically until peaking in early August at values of nearly three. During this peak, fluxes of λE showed a decrease in the late afternoon, suggestive of water stress (Monson et al., 2001). The return of precipitation around day of the year (DOY) 226 and DOY 240–244 brought β back down to values around 1.5 before they increased again through the fall.

In general soil and storage fluxes were much smaller components of the energy budget. Plots of available energy (R_a) versus net radiation (R_{net}) exhibit slopes of 0.92 and 0.96 for the summer and winter, respectively. Of the various storage components, bole storage was the most substantial (Fig. 4c), followed by needle storage. Even though the storage fluxes are much smaller during the winter, bole storage was still the largest contributor. It should be pointed out that both of these fluxes depend on significant approximations. They both rely on accurate scaling up of parameters such as bole temperatures, water content (both boles and needles), which were measured on a small sampling of trees at specific times. Both spatial and temporal variability within the forest likely leads to significant error. However, because the magnitude of these fluxes is small, errors in their estimation do not substantially affect the total energy budget. Storage fluxes do constitute a larger fraction of the available energy at night and errors associated with these fluxes become increasingly important.

Soil heat flux (G) reached a peak value of near $40\,W\,m^{-2}$, typically averaging 15–20 $W\,m^{-2}$ on a half-hourly basis. On average the total heat flux into the soils was about 3% or less of the total energy received by the forest. Small values of the soil heat flux in forested ecosystems are expected based on previous studies (Verma et al., 1986; Baldocchi et al., 1997, Wilson et al., 2001). In winter, the soil heat flux is quite small and negative (-1 to $-4\,W\,m^{-2}$) on a half-hourly basis, with the loss of stored heat from deeper levels toward the surface. G exhibited no diurnal trend during the winter. In fact as the snowpack deepens, diurnal temperature would be expected to change in the top layers of the snowpack (McClung and Schaerer, 1993), suggesting a flux into the snow that was currently unaccounted for in this study. However, due to the low specific heat of ice/snow and preliminary measurements of snowpack temperature profiles during the spring of 2001, this was a small flux and did not substantially impact the overall energy budget. As snowmelt became eminent in spring, G approached zero indicating isothermal conditions at the measurement depth. As soon as snow cover recedes, soil heat flux begins to show its characteristic diurnal pattern, peaking approximately 1 h after the above-canopy R_{net} peaked.

5.2. Seasonal and directional dependence of the energy budget

Energy budget closure was slightly better in the winter than in the summer (0.88 compared to 0.84). This could be due to underestimation of λE as it became more important during the summer months. However, the large changes in Bowen ratio (from 0.7 to 6) accompanied by small changes in energy budget closure over the annual cycle suggests that underestimation must have a small influence. Rather, the seasonal dependence of energy budget closure is more likely the result of increased turbulence intensity during the winter months. As seen in Fig. 7, energy balance approached complete closure at u^* values greater than 1. Improvements in the energy budget with increasing u^* has been noted in past studies (Blanken et al., 1997; Lee, 1998; Mahrt, 1998); although not with the large range of friction velocities noted here. During the winter, neutral, or near-neutral atmospheric stability conditions are observed approximately 70% of the time during which average wind speeds were greater than $6\,m\,s^{-1}$ with correspondingly high u^* values. During the winter, the average day-time u^* was $\sim 0.95\,m\,s^{-1}$, considerably higher than the average day-time summertime value ($\overline{u^*} \sim 0.53\,m\,s^{-1}$).

Upon examining Fig. 7, this change in u^* can easily explain the small improvement in energy balance closure for the winter season.

Less closure was observed during both autumn (0.81 ± 0.02) and spring (0.80 ± 0.01). Springtime deficits were not unexpected since the winter snowpack undergoes melting during this period. Heat used in the conversion of snow to melt-water and subsequent run-off would go undetected with the tower-based measurements. Estimates of the energy required for snow melt were made from weekly measurements of snow water equivalent (SWE) during May 2000. Weekly snow cores of known volume (depth × core area) along an east–west transact were weighed to determine the SWE. Assuming all of the snow lost over a 1 week period was converted to melt-water (and accounting for any added snow over the time period), an average weekly input of $13.0\,\mathrm{MJ\,m^{-2}}$ would be required (designated as the energy required for snowmelt, E_m). This was ∼10% of the weekly integrated net radiation ($\mathrm{Rn_{wk}}$). Addition of this energy to the weekly integrated sensible and latent heat fluxes ($H_\mathrm{wk} + \lambda E_\mathrm{wk}$) resulted in average energy balance closure ($(H_\mathrm{wk} + \lambda E_\mathrm{wk} + E_\mathrm{m})/Rn_\mathrm{wk}$) of 0.92 as opposed to 0.82. This can easily account for the larger springtime energy deficits.

Autumnal energy balance deficits are difficult to understand considering that energy should be released by the freezing of soil water. However, this effect is likely small and mitigated by the appearance of snow coverage before soils have completely frozen. Average daily soil temperatures did not go below freezing until after the yearly snowpack began to develop. It is possible that some of the energy deficit is explained in a similar fashion as spring, as the initial snow cover often melts during subsequent warmer periods in the fall. Once the climate has become cold enough to support continual snowpack, the energy budget deficits lessen. However, these early fall snowfall–snowmelt events are sporadic and difficult to quantify. Therefore, we currently cannot ascertain the specific reason for lower energy budget closure during the fall.

We observed a distinct bias toward lower energy budget closure (∼8–14%) during periods of upslope (easterly) flow. This occurred regardless of season. In fact, the winter–summer differences in energy budget closure may be partially explained by the larger number of upslope periods occurring in the summertime (∼18% compared to ∼8% in winter). Several possibilities for this difference were investigated, including tower effects, inadequate fetch and insufficient turbulent mixing. Tower effects were discounted based on the observation that there was no dependence in the energy budget closure with wind direction within the 60–160° upslope range although the tower should only affect wind directions less than ∼110°.

There is certainly less homogeneous terrain in the eastern direction and the apparent fetch is much shorter; however, these upslope flow events typically occur during the mid- to late-afternoon when surface heating and buoyancy-driven flow should shorten the required fetch. Simple footprint models (Schuepp et al., 1990) suggest that adequate fetch is present during convective upslope flows (90% of flux originates within 600 m). Further evidence suggesting adequate fetch lies in the measurement of sensible heat fluxes as a function of measurement height (between 13.5 and 21.5 m). No vertical flux divergence was observed regardless of wind direction. At the lowest measurement height ($z = 13.5\,\mathrm{m}$, $z/h_\mathrm{c} = 1.18$), the footprint becomes quite compressed (90% of flux within 220 m) indicating that flux contributions are considerably closer to the tower where both topography and forest are relatively uniform. These calculations and observations suggested that inadequate fetch was not the reason for lower energy budget closure during upslope flows.

Upon further scrutiny of the energy budget as a function of wind direction, it became apparent that the difference was most likely related to the lack of adequate turbulent mixing during upslope events. Typical summertime upslope conditions have wind speeds of $\sim 2.5\,\mathrm{m\,s^{-1}}$ and $u^* \sim 0.35\,\mathrm{m\,s^{-1}}$. This contrasts to corresponding downslope conditions ($U \sim 4\,\mathrm{m\,s^{-1}}$ and $u^* \sim 0.6\,\mathrm{m\,s^{-1}}$). As seen in Fig. 7a, there was a distinct difference in the day-time energy balance as u^* increases from 0.3 to $0.6\,\mathrm{m\,s^{-1}}$. Further evidence to support the influence of turbulence intensity was found in the data from downslope and upslope summertime flows as a function of u^*. Fig. 10 shows that during periods of low turbulence ($u^* < 0.45\,\mathrm{m\,s^{-1}}$) and downslope flow, the energy budget closure was similar to that observed during upslope events. There was no observed trend in the energy budget closure with u^* during upslope flows; however, there were statisti-

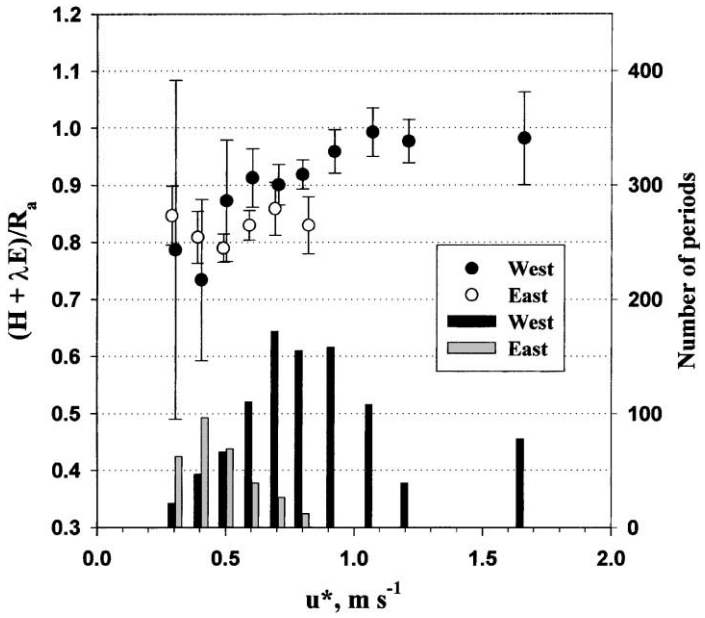

Fig. 10. Plot of the summertime energy balance $((H+\lambda E)/R_a)$ vs. u^* for day-time conditions in the summer of 2000. These are segregated as a function of the two major wind directions: west (downslope, 220–325°) and east (upslope, 60–160°). Data are binned in intervals of $0.1u^*$ for $u^* \leq 0.9\,\mathrm{m\,s^{-1}}$ and $0.15u^*$ for $1.3 > u^* > 0.9\,\mathrm{m\,s^{-1}}$. All data with $u^* > 1.3\,\mathrm{m\,s^{-1}}$ are binned together. Bars at the bottom denote the number of 30 min periods used for each bin.

cally very few upslope periods with $u^* > 0.6\,\mathrm{m\,s^{-1}}$, which are needed to clearly see any increased budget closure. Therefore, it is likely that increased energy budget deficits for easterly wind directions was due to dependence on turbulent mixing, rather than limitations in fetch or tower effects. Lack of adequate turbulence during upslope winds can also lead to increased advection as discussed in Section 5.4.

5.3. Night-time energy balance

Night-time energy balance is significantly affected by atmospheric stability. Under stable stratification and low turbulence, closure of the energy budget is quite poor, and increases only in response to higher turbulence intensity (u^*). This behavior has been observed at other forested sites (Blanken et al., 1997, 1998; Goulden et al., 1997) and results from decoupling of the sub-canopy airflow from the atmosphere above. Cold katabatic drainage airflows beneath the canopy are not detected by the sensors on the tower, resulting in loss of sensible and latent heat flux. Average wind speeds measured at 1 m ($z/h_c = 0.09$) are typically greater than those at 6 m ($z/h_c = 0.53$) during periods with $(z-d)/L > 0.4$. Current experiments are underway to quantify the night-time advective fluxes under stable conditions at our site using profiles of temperature, humidity, wind speed and CO_2 from multiple towers.

As neutral conditions at night are approached and wind speed and friction velocity increase, increased mechanical turbulent transport provides adequate mixing between the airspace within the canopy and the flow above. As a result, sensible heat fluxes measured above the canopy more accurately reflect the surface fluxes and energy balance deficits lessen. However, at very high u^*, sensible heat fluxes showed a substantial decrease (approaching zero) and concurrently, larger energy budget deficits. During these periods, temperature fluctuations become smaller and shifted further towards higher frequencies. It appears that the high frequency temperature fluctuations become too small and cannot be discerned by the sonic anemometer. Conversely, the fluctuations in the wind velocity components (u, v and w) are becoming larger and, thus, not subject to similar limitations. Since noctur-

nal $w'T'$ approaches zero as u^* increases, the noise in the temperature spectrum shown at high frequencies in Fig. 9a must not co-vary with w. Both anemometers exhibited the tendency to miss high frequency temperature flux at night, regardless of the mode of sampling.

During these high wind conditions at night and/or in the winter the latent heat fluxes are small ($<40\,\mathrm{W\,m^{-2}}$). This results in considerable noise in the q power spectra regardless of wind speed. Although difficult to say with great certainty, it appears that the lack of resolution encountered with the sonic temperature is also present in the Kr hygrometer time series for water vapor density. This would be understandable as the magnitude of the water vapor fluctuations should also be diminishing at high u^*.

5.4. Evaluation of the energy budget deficit

Figs. 6 and 7 show that we often obtain energy balance of better than 80% based on half-hourly flux measurements. Closure of between 75 and 95% is typical on the half-hourly basis, with an average of about 0.85. This depends largely on the degree of turbulence present. With a few exceptions (Verma et al., 1986; Kelliher et al., 1993), closure of the energy budget is typically not observed on the half-hourly time scale at many forested eddy flux sites (Lee and Black, 1993; Goulden et al., 1996, 1997; Blanken et al., 1997, 1998; Mahrt, 1998; Anthoni et al., 1999; Aubinet et al., 2000; Wilson et al., 2001). Although our site is characterized by sloped terrain, a complex canopy, and nearby mountains that can cause complex flow patterns to develop, the measured energy budget deficits are similar to the latter studies.

The reasons for lack of closure across sites are not completely understood, but the following possibilities are suspected (Stannard et al., 1994; Mahrt, 1998; Aubinet et al., 2000; Twine et al., 2000; Wilson et al., 2001): (1) systematic instrument error, (2) mismatch of footprints of turbulent and non-turbulent fluxes, (3) neglected terms in the energy budget, (4) loss of turbulent flux contributions at either high or low frequency, and (5) mean advection (either vertical or horizontal) of scalar quantities. It is likely that contributions from all five possible biases can contribute to the observed energy budget deficit to some degree, although in varying magnitude.

We have investigated the possibilities of systematic errors due to the measuring systems at our site. Intercomparisons between two different sonic anemometers (providing independent temperature measurements) and two different water vapor instruments revealed excellent agreement. These intercomparisons covered a large range of meteorological conditions (wind speeds, temperatures) and varying Bowen ratios ($\beta = 0.7$–6). Therefore, it seems unlikely that the deficit can be explained by a bias in one of the turbulent flux instruments. It is also unlikely that improper measurement of net radiation during the day is responsible for the energy imbalance, since both the CNR-1 and the REBS Q*7.1 were in relatively good agreement over the extent of the study. We note a distinct discrepancy in the long-wave sensitivity of the two radiometers. Further tests are needed to determine the nature of this difference.

Mismatch of flux footprints between the non-turbulent and turbulent fluxes has been discussed previously by Schmid (1997). It is quite apparent that source areas for eddy covariance measurements are not equivalent to those of the net radiometer, soil heat flux plates, or storage fluxes. The forest contains considerable heterogeneity (Monson et al., 2001) that should lead to some degree of footprint mismatch. Currently we are unable to describe the spatial variability of the available energy components over the entire fetch of the turbulent fluxes; however, previous studies (Stannard et al., 1994; Twine et al., 2000) have shown that net radiation (which constitutes the largest fraction of available energy) shows little spatial variability over both uniform and patchy surfaces. These studies and others (Mahrt, 1998; Wilson et al., 2001) looking across multiple sites conclude that it is unlikely that footprint mismatch would consistently lead to a shortfall of energy in the turbulent sensible and latent heat fluxes.

These same studies (Mahrt, 1998; Wilson et al., 2001) have also reasoned that it is unlikely that there are significant energy terms missing from the budget equation. In the current study, the storage or release of heat above the soil heat flux plates, and in the snowpack were not measured. However, periodic estimation of this flux was made and observed to be small ($<$1–2% of the net radiation). Paw U et al. (2000) have suggested an energy correction term due to the expansion of air during evaporation at a constant

pressure. Their work suggests an energy correction to the turbulent fluxes of about 7–8% of the latent heat flux. Although significant, it is likely less important at our site, since Bowen ratios are rarely less than unity and often greater than 3 during winter. This correction would be, at most, ~3% of R_a at our site and negligible during the wintertime. It is possible that this correction could be partially responsible for the winter–summer differences described in the Section 5.3.

We have estimated the flux loss at high frequencies due to sensor separation, line averaging and tubing attenuation and found that these are all too small to explain the observed shortfall. High frequency losses due to tubing attenuation tend to be most important at high wind speeds when the co-spectral densities shift to higher frequencies. However, we observed better energy budget closure under these conditions during the day-time. The excellent agreement between the open- and closed-path sensors (which have different degrees of high-pass filtering) suggests that losses of high frequency flux contributions are small.

The loss of low frequency flux caused by using too short of a sampling period has been suggested to contribute to the lack of energy budget closure in many instances (Mahrt, 1998). Low frequency flux contributions include elongation of eddies in the downwind direction (Mahrt, 1998), formation of large-scale roll vortices (LeMone, 1973), or quasi-stationary eddies (Lee and Black, 1993) which pass the sampling site at time scales longer than the 30 min sampling time. Diurnal patterns of sensible and latent heat fluxes on clear days often show a "saw-tooth" pattern (data not shown), even though the diurnal pattern of net radiation exhibits a smooth curve. Variations in sensible and latent heat flux during these times show a positive correlation, suggesting that changes in energy partitioning are not responsible. Such diurnal patterns have been observed and discussed previously (Lee and Black, 1993; Blanken et al., 1997) where they were attributed to the presence of large-scale turbulent features which are undersampled at the half-hourly time scale.

Occurrence of low frequency effects are also evident in the dependence of the energy balance on friction velocity and corresponding co-spectra. Fig. 7a indicates a slow gradual improvement in closure with increasing u^*. Correspondingly, co-spectra of $w'T'$ suggest that the peak frequencies for flux

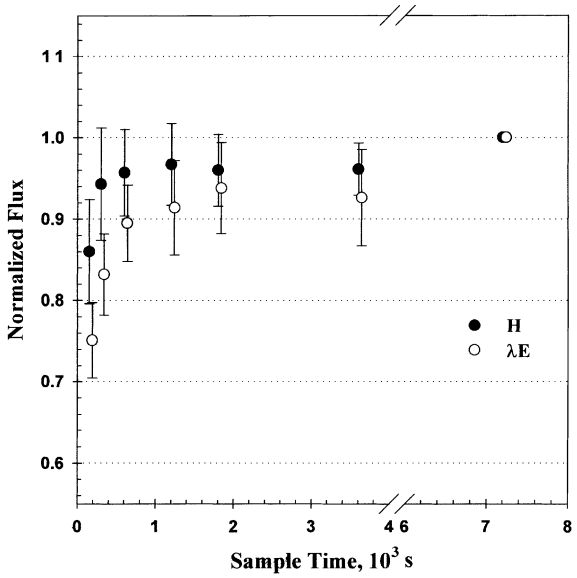

Fig. 11. Plots of the average day-time ($R_{net} > 10\,W\,m^{-2}$) fluxes of sensible and latent heat during July 2000 for various averaging times, ranging from 2.5 min to 2 h. Fluxes within a given 2 h time period were averaged and then normalized to the flux computed for whole 2 h sampling period (assuming that this averaging time captures all the low frequency flux contributions). Data are the average of 14 days of flux measurements in July 2000, and error bars are the normalized S.E. of all the 2 h samples.

transport shift from 0.04–0.05 to 0.1–0.2 Hz during these high wind speed events (see Figs. 3 and 9). Possibly more significant, low frequency contributions ($f < 0.01$ Hz) decrease substantially at high u^* values. This suggests that large-scale motions are "broken up" during high turbulence periods as the thermally-induced transport is dampened and mechanically-derived turbulence dominates. Thus, substantially more energy or mass is transported by eddies within a frequency range that is sufficiently characterized within the 30 min sampling period.

To further investigate this possibility, sampling time was varied between 2.5 min and 2 h during typical day-time summertime conditions. Fig. 11 shows the effect on the average sensible and latent fluxes for various sampling periods (all normalized to the 2 h flux). At sampling times of 30 min, approximately 96 and 94% of the 2 h sensible and latent heat fluxes are obtained, respectively. At the time of the calculations (summer of 2000) and using an average Bowen ratio

of 1.5, one can derive an underestimate of ∼5% in the energy budget using the 30 min time averages. Although not negligible, this does not fully explain the 10–18% gap in overall energy budget closure.

The formation of both horizontal and/or vertical advective fluxes is one further explanation for the lack of energy budget closure observed. In fact, according to the models of scalar transfer over hills proposed by Raupach et al. (1992) and Raupach and Finnigan (1997), these advective fluxes should be expected on sloped sites such as ours. This is due to variability in radiation, soil water content, and biophysical properties of the vegetation along the slope, and from perturbations to the flow field due to topography. Since our analysis currently only measures the vertical turbulent flux (assumes horizontal homogeneity), these advective components of the flux go unobserved. The measurement of advective flux components from a single tower is currently a topic of considerable concern (Lee, 1998; Finnigan, 1999; Baldocchi et al., 2000; Paw U et al., 2000). Lee (1998) revisited the basic conservation equation and, assuming no horizontal flux divergence and no horizontal advection, derived an expression that was used to calculate the vertical advective flux of a scalar, x:

$$F_{\mathrm{va}}(x) = \bar{w}_r(\bar{x}_r - \langle\bar{x}\rangle) \tag{7}$$

In Eq. (7), the subscript r denotes a quantity at height z, following the notation of Lee (1998). The vertical advective flux (F_{va}) is a function of a mean vertical velocity ($\bar{w}_r$) and the difference between the scalar concentration at z_r and the average scalar concentration between this height and the ground ($\langle\bar{x}\rangle$). The mean vertical velocity was determined by rotating the co-ordinate system to one where vertical velocity is normal to the local terrain surface (as opposed to the standard procedure of rotating $\bar{w}$ to zero). As explained by Lee (1998) and further exemplified by Baldocchi et al. (2000), practical implementation of Eq. (7) to 30 min flux data is problematic. Uncertainties in $\bar{w}_r$ are considerable and sensor biases can lead to significant error in the scalar differences. There is also considerable debate over the validity of assuming no horizontal advection or flux divergence in complex topography (Finnigan, 1999; Baldocchi et al., 2000).

We reevaluated sensible heat fluxes from 2 months (July 2000 and January 2001) by rotating the co-ordinate system in the u–w plane according to the regression line shown in Fig. 1b. This allows for calculation of a mean vertical velocity ($\bar{w}_r$). Temperature differences were computed using the measured gradient of temperature at 2 and 21.5 m. Although there was considerable scatter in the computed advective sensible heat flux, H_{va}, some qualitative observations were noted. Vertical advective fluxes for sensible heat were larger at low u^* ($<0.8\,\mathrm{m\,s^{-1}}$). At high friction velocities, temperature gradients became small and H_{va} approached zero. These conditions are often observed during winter downslope winds, where day-time energy budget closure approached unity. As described by Lee (1998) and Baldocchi et al. (2000), one particular situation where the vertical advection flux term is likely to be significant (and horizontal contributions to advection may cancel out) is under highly convective conditions with low wind speed. These conditions are often met during periods of upslope flow. As described previously, these are also periods which exhibit lower energy budget closure. Therefore, it qualitatively appears that advective fluxes likely play a significant role in the lack of energy balance closure at this site. Multiple tower measurements or advances in theory are needed to further address their magnitude. However, it is interesting to note that even though the Niwot Ridge site rests in a very complicated location (sloped terrain, complex canopy, nearby mountains) the energy budget deficit is comparable with many other forested ecosystem sites. This suggests that these advective effects could be somewhat universal over tall canopies, although further evidence is needed.

6. Conclusions

We have measured the energy balance over a subalpine coniferous forest in complex (mountainous) terrain during two annual cycles. A high degree of closure was only observed during day-time periods of high turbulence ($u^* > 1\,\mathrm{m\,s^{-1}}$). At lower friction velocities, day-time energy budget closure was typically 80–90%, which is typical of many other forested sites. Nocturnal energy budget closure was highly dependent on stability. At low u^*, the canopy airspace becomes decoupled from the airflow above, and turbulent fluxes measured above the canopy no longer reflect the surface fluxes.

The dependence of day-time budget closure on u^* appears to be due to two major factors: (1) the decrease in low frequency contributions to the measured flux during periods of high turbulence, and (2) increased mixing at high u^* values. Higher wind speeds and turbulence led to a co-spectral shift toward higher frequencies, and this results in an increasing portion of the flux carried by frequencies that were more adequately measured using a 30 min time average. Furthermore, these periods tend to enhance both horizontal and vertical mixing. This creates a more homogeneous surface layer, which, in turn, yields single point measurements (i.e. from the tower) that are more representative of the surrounding ecosystem. During low turbulence periods, large quasi-stationary convective structures can be formed which have the possibility of creating vertical and horizontal advective fluxes. These go unaccounted for in vertical turbulent flux measurements above the canopy. Currently, we are unable to confidently calculate these advective contributions; however, temperature gradient measurements suggest that any vertical advective contribution is minimized at high u^* values where energy budget closure is often attained. Although not definitive, these observations suggest contributions from advective fluxes. The lack of complete closure that we observed is typical of other forested ecosystems, regardless of topography. This suggests that advective flux components are likely ubiquitous in the surface boundary layer and need to be measured in future studies of surface–atmosphere exchange and the energy budget.

Acknowledgements

The authors would like to thank the other members of the Monson research group for their assistance and contributions. Dr. Jed Sparks and Kim Sparks provided much of the biometric data; Laura Scott-Denton provided soil moisture data. Dr. David Stannard of the US Geological Survey provided helpful discussions. Dr. Dave Bowling provided invaluable help during early stages of the project. The authors would also like to thank members of the ATD of the NCAR for assistance and guidance in establishing this research site and the data acquisition system. Special thanks are offered to Dr. Tony Delany, Gordon McLean, and Dr. Steve Oncley for their time and efforts. The authors would also like to thank Dr. Bill Bowman and staff at the University of Colorado Mountain Research Station and the Niwot Ridge Long-Term Ecological Research (LTER) site. Finally, we would like to thank the US Forest Service for permitting the establishment of the research site in the Roosevelt National Forest. This research was funded by the South Central Section of the National Institute for Global Environmental Change (NIGEC) through the U.S. Department of Energy and, in part, by the National Science Foundation.

References

Anthoni, P.M., Law, B.E., Unsworth, M.H., 1999. Carbon and water vapor exchange of an open-canopied ponderosa pine ecosystem. Agric. For. Meteorol. 95, 151–168.

Aubinet, M., Grelle, A., Ibrom, A., Rannik, U., Moncrieff, J., Foken, Th., Kowalski, P., Martin, P., Berbigier, P., Bernhofer, Ch., Clement, R., Elbers, J., Granier, A., Grunwald, T., Morgenster, K., Pilegaard, K., Rebmann, C., Snijders, W., Valentini, R., Vesala, T., 2000. Estimates of the annual net carbon and water exchanges of European forests: the EUROFLUX methodology. Adv. Ecol. Res. 30, 113-114.

Baldocchi, D.D., Finnigan, J., Wilson, K., Paw U, K.T., Falge, E., 2000. On measuring net ecosystem carbon exchange over tall vegetation on complex terrain. Boundary Layer Meteorol. 96, 257–291.

Baldocchi, D.D., Vogel, C.A., Hall, B., 1997. Seasonal variation of energy and water vapor exchange rates above and below a boreal jack pine canopy. J. Geophys. Res. 102, 28939–28951.

Barry, R.G., 1973. A climatological transact on the east slope of the Colorado Front Range. Arct. Alp. Res. 5, 89–110.

Barry, R.G., 1993. Mountain Weather and Climate. Metheun & Co., New York.

Blanken, P.D., Black, T.A., Yang, P.C., Neumann, H.H., Nesic, Z., Staebler, R., den Hartog, G., Novak, M.D., Lee, X., 1997. Energy balance and canopy conductance of a boreal aspen forest: partitioning overstory and understory components. J. Geophys. Res. 102, 28915–28927.

Blanken, P.D., Black, T.A., Neumann, H.H., den Hartog, G., Yang, P.C., Nesic, Z., Staebler, R., Chen, W., Novak, M.D., 1998. Turbulent flux measurements above and below the overstory of a boreal aspen forest. Boundary Layer Meteorol. 89, 109–140.

Brazel, A., Brazel, P., 1983. Summer diurnal wind patterns at Niwot Ridge, CO.. Phys. Geog. 4, 53–61.

Businger, J.A., Dabberdt, W.F., Delany, A.C., Horst, T.W., Martin, C.L., Oncley, S.P., Semmer, S.R., 1990. The NCAR atmosphere-surface turbulent exchange research (ASTER) facility. Bull. Am. Meteorol. Soc. 71, 1006–1011.

Dunlap, F., 1912. The specific heat of wood. USDA For. Survey Bull. 110, 1–28.

Fitzjarrald, D.R., Moore, K.E., 1994. Growing season boundary layer climate and surface exchanges in a subarctic lichen woodland. J. Geophys. Res. 99, 1899–1917.

Finnigan, J., 1999. A comment on the paper by Lee (1998): on micrometeorological observations of surface–air exchange over tall vegetation. Agric. For. Meteorol. 97, 55–64.

Foken, Th., Wichura, B., 1996. Tools for the quality assessment of surface-based flux measurements. Agric. For. Meteorol. 78, 83–105.

Ganster, J., Fink, H.-P., 1999. Physical constants of cellulose. In: Brandup, J., Immergut, E.H., Grulke, E.A. (Eds.), Polymer Handbook, 4th Edition. Wiley, New York, pp. 135–157.

Goulden, M.J., Munger, J.W., Fan, S.-M., Daube, B.C., Wofsy, S.C., 1996. Measurement of carbon sequestration by long-term eddy covariance: methods and critical evaluation of accuracy. Global Change Biol. 22, 169–182.

Goulden, M.J., Daube, B.C., Fan, S.-M., Sutton, D.J., Bazzaz, A., Munger, J.W., Wofsy, S.C., 1997. Physiological responses of a black spruce forest to weather. J. Geophys. Res. 102, 28987–28996.

Greco, S., Baldocchi, D.D., 1996. Seasonal variations of CO_2 and water vapor exchange rates over a temperate deciduous forest. Global Change Biol. 2, 183–198.

Hollinger, D.Y., Wofsy, S.C., 1997. Science Plan for AmeriFlux: Long-term Flux Measurement Network of the Americas. http//www.esd.ornl.gov/programs/NIGEC/scif.html .

Jarvis, P.G., James, G.B., Landsberg, J.J., 1976. Coniferous forests. In: Monteith, J.L. (Ed.),Vegetation and the Atmosphere, Vol. 2. Academic Press, San Diego, pp. 171–240.

Jarvis, P.G., Massheder, J.M., Hale, S.E., Moncrieff, J.B., Rayment, M., Scott, S.L., 1997. Seasonal variation of carbon dioxide, water vapor, and energy exchanges of a boreal black spruce forest. J. Geophy. Res. 102, 28953–28966.

Kaimal, J.C., Finnigan, J.J., 1994. Atmospheric Boundary Layer Flows: Their Structure and Measurement. Oxford University Press, Oxford.

Kelliher, F.M., Köstner, B.M.M., Hollinger, D.Y., Byers, J.N., Hunt, J.E., McSeveny, T.M., Meserth, R., Weir, P.L., Schulze, E.-D., 1993. Evaporation, xylem sap flow, and tree transpiration in a New Zealand broad-leaved forest. Agric. For. Meteorol. 62, 53–73.

Laubach, J., Raschendorfer, M., Kreilein, H., Gravenhorst, G., 1994. Determination of heat and water vapor fluxes above a spruce forest by eddy correlation. Agric. For. Meteorol. 71, 373–401.

Lee, X., 1998. On micrometeorological observations of surface–air exchange over tall vegetation. Agric. For. Meteorol. 91, 39–49.

Lee, X., Black, T.A., 1993. Atmospheric turbulence within and above a Douglas-fir stand. Part II. Eddy fluxes of sensible heat and water vapor. Boundary Layer Meteorol. 64, 369–389.

LeMone, M.A., 1973. The structure and dynamics of horizontal roll vortices in the planetary boundary layer. J. Atmos. Sci. 30, 1308–1320.

Lenshow, D.H., Raupach, M.R., 1991. The attenuation of fluctuations in scalar concentrations through sampling tubes. J. Geophys. Res. 96, 5259–5268.

Leuning, R., Judd, M.J., 1996. The relative merits of open- and closed-path analysers for measurement of eddy fluxes. Global Change Biol. 2, 241–253.

Leuning, R., King, K.M., 1992. Comparison of eddy-covariance measurements of CO_2 fluxes by open- and closed-path CO_2 analyzers. Boundary Layer Meteorol. 59, 297–311.

Lindroth, A., 1985. Seasonal and diurnal variation of energy budget components in coniferous forests. J. Hydrol. 82, 1–15.

Mahrt, L., 1998. Flux sampling errors for aircraft and towers. J. Ocean Atmos. Tech. 15, 416–429.

Marshall, D.C., 1958. Measurement of sap flow in coniferous by heat transport. Plant Physiol. 33, 385–396.

Massman, W.J., 2000. A simple method for estimating frequency corrections for eddy covariance systems. Agric. For. Meteorol. 104, 185–198.

McClung, D., Schaerer, 1993. The Avalanche Handbook. The Mountaineers, Seattle, p. 272.

Monson, R.K., Turnipseed, A.A., Sparks, J.P., Harley, P.C., Scott-Denton, L.E., Sparks, K., Huxman, T.E., 2001. Carbon sequestration in a high-elevation subalpine forest, Global Change Biol., in press.

Moore, C.J., 1986. Frequency response corrections for eddy correlation systems. Boundary Layer Meteorol. 37, 17–35.

Oke, T.R., 1987. Boundary Layer Climates. Methuen & Co., New York.

Parrish, D.D., Hahn, C.H., Fahey, D.W., Williams, E.J., Bollinger, M.J., Hubler, G., Buhr, M.P., Murphy, P.C., Trainer, M., Hsie, E.Y., Liu, S.C., Fehsenfeld, F.C., 1990. Systematic variations in the concentrations of NO_x (NO Plus NO_2) at Niwot Ridge, Colorado. J. Geophys. Res. 95, 1817–1836.

Paw U, K.T., Baldocchi, D.D., Meyers, T.P., Wilson, K.B., 2000. Correction of eddy-covariance measurements incorporating both advective effects and density fluxes. Boundary Layer Meteorol. 97, 487–511.

Raupach, M.R., Weng, W.S., Carruthers, D.J., Hunt, J.C.R., 1992. Temperature and humidity fields and fluxes over low hills. Quart. J. Roy. Meteorol. Soc. 118, 191–225.

Raupach, M.R., Finnigan, J.J., 1997. The influence of topography on meteorological variables and surface–atmosphere interactions. J. Hydrol. 190, 182–213.

Schmid, H.P., 1997. Experimental design for flux measurements: matching scales of observation and fluxes. Agric. For. Meteorol. 87, 179–200.

Schotanus, P., Nieuwstadt, F.T.M., De Bruin, H.A.R., 1983. Temperature measurement with a sonic anemometer and its application to heat and moisture fluxes. Boundary Layer Meteorol. 26, 81–93.

Schuepp, P.H., Leclerc, M.Y., MacPherson, J.I., Desjardins, R.L., 1990. Footprint prediction of scalar fluxes from analytical solutions of the diffusion equation. Boundary Layer Meteorol. 50, 355–373.

Stannard, D.I., Blanford, J.H., Kustas, W.P., Nichols, W.D., Amer, S.A., Schmugge, T.J., Welts, M.A., 1994. Interpretation of surface flux measurements in heterogeneous terrain during the Monsoon'90 experiment. Water Resource Res. 30, 1227–1239.

Stull, R.B., 1988. An Introduction to Boundary Layer Meteorology. Kluwer Academic Publishers, Dordrecht.

Twine, T.E., Kustas, W.P., Norman, J.M., Cook, D.R., Houser, P.R., Meyers, T.P., Prueger, J.H., Starks, P.J., Wesely, M.L., 2000. Correcting eddy-covariance underestimates over a grassland. Agric. For. Meteorol. 103, 279–300.

Verma, S.B., Baldocchi, D.D., Anderson, D.E., Matt, D.R., Clement, R.J., 1986. Eddy fluxes of CO_2, water vapor, and sensible heat over a deciduous forest. Boundary Layer Meteorol. 36, 71–91.

Webb, E.K., Pearman, G.I., Leuning, R., 1980. Correction of flux measurements for density effects due to heat and water vapor transfer. Quart. J. Roy. Meteorol. Soc. 106, 85–100.

Wilson, K., Goldstein, A., Falge, E., Aubinet, M., Baldocchi, D.D., Bernhofer, C., Ceulemans, R., Dolman, H., Field, C., Grelle, A., Law, B., Loustau, D., Meyers, T., Moncrieff, J., Monson, R., Oechel, W., Tenhunen, J., Valentini, R., Verma, S., 2001. Energy balance closure at FLUXNET sites. Agric. For. Meteorol, in press.